

# Optical pumping of alkali-metal vapor with hyperfine-resolved buffer gas pressure

Kezheng Yan,<sup>1</sup> Jinbo Hu,<sup>1</sup> and Nan Zhao<sup>1,\*</sup>

<sup>1</sup>*Beijing Computational Science Research Center*

(Dated: March 9, 2026)

Optical pumping is fundamental to high-precision measurement using thermal alkali-metal atoms in vapor cells. In applications such as spin-exchange-relaxation-free magnetometers, buffer gases (e.g., N<sub>2</sub> or He) are commonly employed to quench fluorescence and mitigate wall relaxation. In the high-pressure limit (e.g., the N<sub>2</sub> pressure  $p_{\text{N}_2} > 1$  atm), where collisional broadening exceeds the hyperfine splitting of the alkali-metal atoms, optical pumping theory provides a clear description of the angular momentum exchange between photons and atomic spins. However, in many magnetic sensing scenarios, this high-pressure condition is not strictly satisfied, rendering the high-pressure approximation inaccurate. Consequently, a precise quantitative understanding of optical pumping under realistic pressures is critical for determining optimal buffer gas parameters, selecting operating points (e.g., pump frequency and intensity), and enhancing system reliability and stability. To address this, we develop a theory of optical pumping in the quasi-high-pressure regime, where collisional broadening is comparable to the ground-state hyperfine splitting. We demonstrate that optical absorption, spin polarization, and magnetic resonance linewidth in this regime differ significantly from those predicted by the high-pressure limit. Our study extends conventional modeling and offers critical guidance for atomic magnetometry operating under realistic buffer gas pressures.

## I. INTRODUCTION

Optical pumping of alkali-metal atoms serves as the foundation for a wide array of quantum sensing technologies, ranging from atomic clocks [1, 2] to magnetometers [3–5] and inertial sensors [6–8]. In particular, atomic magnetometers exploit the spin dynamics of alkali-metal atoms to achieve ultra-sensitive field detection. In this process, a circularly polarized light beam creates atomic spin polarization, which then precesses at the Larmor frequency in an external magnetic field, providing a precise measure of the field strength.

Vapor cells used in these applications are generally categorized as either evacuated or buffer-gas-filled [9]. While evacuated cells rely on anti-relaxation coatings to prevent wall-collision relaxation [10, 11], buffer-gas-filled cells utilize inert gases to modify atomic diffusion and quench fluorescence [12, 13]. These features allow operation at higher temperatures and atomic densities, enabling the ultra-high sensitivity characteristic of modern magnetometers [14, 15]. This work focuses specifically on the optical pumping dynamics within such buffer-gas-filled cells.

Depending on the buffer gas pressure, optical pumping operates in distinct regimes, yet a comprehensive theoretical framework covering the intermediate pressures is currently lacking. In the low-pressure (LP) regime with typical buffer gas pressure  $\lesssim 10$  Torr, strong and narrow optical resonances of well resolved hyperfine multiplets enables refined optical manipulation, such as in atomic clocks based on coherent population trapping (CPT) [16]. In the high-pressure (HP) limit (e.g., buffer gas pressure  $> 1$  atm), strong collisional quenching and pressure broadening dominate [17–19]. This treatment renders hyperfine multiplets unresolved and forms the basis of the spin-temperature distribution (STD) widely used in, e.g., spin-exchange relaxation free (SERF) magnetometers

[20, 21]. However, many optical pumping systems including atomic magnetometers operate in the quasi-high-pressure (QHP) regime (typically  $\sim 10^2$  Torr). We focus on this intermediate regime, in which the ground-state (GS) hyperfine structure remains spectrally resolvable while the excited-state (ES) structure is unresolved. This leads to spin dynamics that are neither fully captured by the LP models nor the simplified HP approximations. Developing a precise quantitative understanding of the QHP regime is therefore critical. It not only enables the determination of optimal operating points to maximize sensitivity, but also facilitates the assessment of long-term system stability against parameter drifts.

The spectral resolvability of the GS hyperfine structure fundamentally governs the optical pumping process in the QHP regime. Unlike the HP limit, the QHP regime requires a rigorous treatment of the resolvable multiplets and their distinct contributions to absorption. Starting from the master equation in Liouville space, we incorporate the electric-dipole interaction and relevant collisional mechanisms to derive the mathematical form of optical pumping in the QHP regime. Crucially, we establish a compact relation linking QHP superoperators to their HP counterparts, providing a unified theoretical framework that facilitates both physical analysis and efficient numerical evaluation.

A distinct feature of the QHP regime is the dependence of the absorption cross-section on pumping-light polarization and intensity, which markedly differs from the HP limit. Within our framework, we derive analytical expressions for absorption under both linearly and circularly polarized pumping. We elucidate how the intensity-dependent redistribution of population among hyperfine multiplets reshapes the detuning response of the absorption behavior.

Consequently, the steady-state atomic population in the QHP regime generally deviates from the standard STD. We demonstrate that while the STD can approximate the distribution shape under strong spin-exchange collisions, the effective temperature parameter—namely the spin polarization—requires QHP-specific corrections. Our numerical re-

\* [nzhao@csrc.ac.cn](mailto:nzhao@csrc.ac.cn)

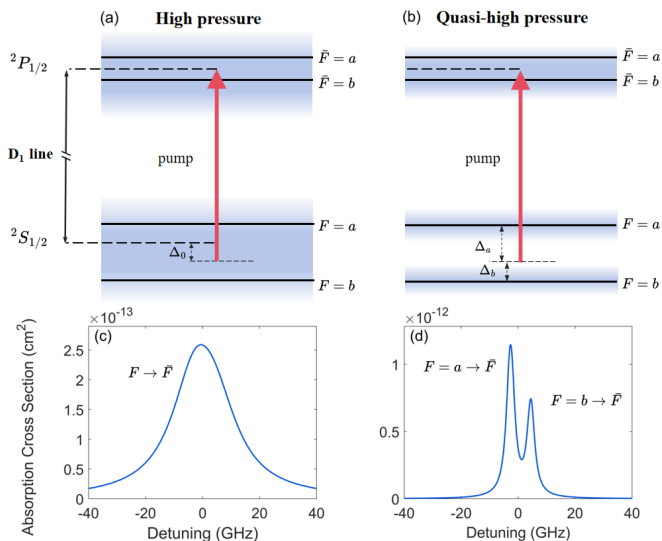


FIG. 1. Schematic illustration of optical pumping on the alkali-metal D<sub>1</sub> line in the HP limit and QHP regime. (a) and (b) show the GS and ES hyperfine multiplets, with different collisional broadening  $\Gamma_{\text{brd}}$  illustrated by blue level edges. Each of  $F$  and  $\bar{F}$  corresponds to either  $a = I + 1/2$  or  $b = I - 1/2$  for nuclear spin  $I$ . Laser detuning from the D<sub>1</sub> line reference frequency is denoted by  $\Delta_0$ , while  $\Delta_F$  for  $F = a$  and  $b$  are the detunings corrected from  $\Delta_0$  by the GS hyperfine splitting. (c) and (d) present the corresponding absorption cross section  $\sigma_0$  for unpolarized  $^{87}\text{Rb}$ , with  $\Gamma_{\text{brd}} = 3, 20$  GHz, respectively. The hyperfine splittings are  $\omega_{\text{hf}}^{(g)} = 6.8$  GHz and  $\omega_{\text{hf}}^{(g)} = 0.81$  GHz. Collisional shifts are not included for simplicity. Absorption peaks corresponding to different  $F \rightarrow \bar{F}$  transitions are indicated. Doppler broadening  $\Gamma_{\text{dop}} = 0.57$  GHz is included using the Voigt profile, which is negligible in the two regimes.

sults regarding spin polarization versus pumping power and frequency reveal that resonant pumping at specific hyperfine levels can yield larger steady-state spin polarization.

Beyond fundamental spin dynamics, we analyze the magnetic-resonance linewidth to identify optimal operating conditions for atomic magnetometers. We find that resonant pumping at the lower hyperfine-split levels not only enhances spin polarization but also yields a favorable magnetic-resonance linewidth. This suggests a strategy for optimizing sensitivity through simultaneous improvements in resonance amplitude and linewidth.

The remainder of this paper is organized as follows. Section II defines the QHP regimes based on spectral characteristics. Section III presents the theoretical framework based on the Liouville space master equation. Section IV discusses the unique features of absorption, spin polarization, and magnetic resonance linewidth in the QHP regime. Finally, Section V summarizes the main findings.

## II. REGIMES OF BUFFER GAS PRESSURE

Optical pumping in alkali-metal vapor relies on the coupling between GS and ES of the atomic D line transition, which drives atoms toward a targeted state via optical excita-

tion and collisional relaxation. The D<sub>1</sub> line typically serves as the model system, as shown in Fig. 1, where  $F$  and  $\bar{F}$  denote the angular momentum of the GS and ES hyperfine multiplets, respectively. While light absorption initiates the pumping process, the spectral characteristics are governed by line broadening mechanisms. In buffer-gas vapor cells, which are the focus of this work, collisional broadening  $\Gamma_{\text{brd}}$  dominates, serving as the primary criterion for distinguishing pressure regimes.

To characterize these regimes, we analyze the absorption cross-section for unpolarized atoms,  $\sigma_0$ , in the limit of vanishing photon flux  $\Phi$  of the incident laser beam (i.e.,  $\Phi \rightarrow 0$ ). In the LP regime,  $\Gamma_{\text{brd}}$  is insufficient to bridge the ES or GS hyperfine splitting, and dynamics are further complicated by radiation trapping [13] and atomic diffusion [22]. Instead of this regime, we focus on the distinction between the HP limit and the QHP regime in the following. In the HP limit,  $\Gamma_{\text{brd}}$  is sufficiently large to merge all GS and ES hyperfine splittings into a single resonance peak, as depicted in Figs. 1(a) and 1(c). Here, the system simplifies significantly, and underlies the STD [20, 21].

The QHP regime represents an intermediate condition where  $\Gamma_{\text{brd}}$  is comparable to the GS hyperfine splitting but significantly larger than that of the ES. Figures 1(b) and 1(d) illustrate that the absorption profile simplifies to two resolved components associated with the GS multiplets  $F = a$  and  $b$ . Unlike the HP limit, where atoms in different multiplets absorb photons at an almost common rate, in the QHP regime, the pumping process becomes more sensitive to the pump laser frequency. Furthermore, stronger pump light significantly alters the population distribution between the  $a$  and  $b$  levels, which in turn reshapes the absorption behavior and spin polarization—factors critical for subsequent applications.

While the linear absorption profile in the  $\Phi \rightarrow 0$  limit serves as a convenient classification metric, the rich physical phenomena emerging at higher optical intensities are the primary focus of this work. We emphasize that the behaviors in the QHP regime cannot be fully described by the simple optical pumping model used in the HP limit. Therefore, a key contribution of this paper is the development of a unified theoretical framework capable of treating the continuous transition from the HP limit to the QHP regime. The following sections will present this unified approach and analyze the spin evolution in practical scenarios, such as atomic magnetometers, where operation often spans these intermediate pressure conditions.

## III. THEORETICAL TREATMENT

### A. Master equation in Liouville space

We study the spin dynamics of optically pumped alkali-metal atoms in vapor cells, where both coherent and incoherent processes contribute to the evolution of the atomic ensemble.

ble. For the coherent part, the atomic spin Hamiltonian is [9]

$$H_0 = \frac{\omega^{(\text{eg})}}{2} (1^{(\text{e})} - 1^{(\text{g})}) + H^{(\text{g})} + H^{(\text{e})}, \quad (1)$$

$$H^{(\text{g})} = \sum_{F, m_F} \omega_{F, m_F}^{(\text{g})} |F, m_F\rangle \langle F, m_F|, \quad (2)$$

$$H^{(\text{e})} = \sum_{\bar{F}, \bar{m}_F} \omega_{\bar{F}, \bar{m}_F}^{(\text{e})} |\bar{F}, \bar{m}_F\rangle \langle \bar{F}, \bar{m}_F|, \quad (3)$$

where  $1^{(\text{g})}$  and  $1^{(\text{e})}$  are identity operators of the GS and ES subspaces, respectively, and  $\omega^{(\text{eg})}$  denotes the reference frequency of the optical transition. In Eqns. (2) & (3), the Hamiltonians  $H^{(\text{g})}$  and  $H^{(\text{e})}$  are expressed in their eigen-representations with eigen-frequencies  $\omega_{F, m_F}^{(\text{g})}$  and  $\omega_{\bar{F}, \bar{m}_F}^{(\text{e})}$ , together with the eigenstates  $|F, m_F\rangle$  and  $|\bar{F}, \bar{m}_F\rangle$ , respectively, with  $F$  ( $\bar{F}$ ) being the total angular momentum quantum number, and  $m_F$  ( $\bar{m}_F$ ) being the magnetic quantum number.

Having specified the atomic Hamiltonian  $H_0$ , we introduce the light-atom interaction Hamiltonian  $H_{\text{int}}$ , which takes an electric-dipole form [9]

$$H_{\text{int}} = V + V^\dagger = -\Omega_{\text{I}} \mathbf{d}^\dagger \cdot \hat{\mathbf{e}} - \Omega_{\text{I}}^* \mathbf{d} \cdot \hat{\mathbf{e}}^*, \quad (4)$$

with  $V$  describing photon absorption and atom excitation with optical Rabi frequency  $\Omega_{\text{I}}$ , and  $V^\dagger$  representing the reverse process. Here,  $\mathbf{d}$  denotes the dimensionless dipole operators, and  $\hat{\mathbf{e}}$  is the unit vector of the positive-frequency classical electric field. For a monochromatic laser beam with frequency  $\omega$ , the laser detuning with respect to the atomic transition  $|F, m_F\rangle \leftrightarrow |\bar{F}, \bar{m}_F\rangle$  is

$$\Delta_{\bar{F}\bar{m}_F, Fm_F} = \Delta_0 - \left( \omega_{\bar{F}, \bar{m}_F}^{(\text{e})} - \omega_{F, m_F}^{(\text{g})} \right), \quad (5)$$

where  $\Delta_0 = \omega - \omega^{(\text{eg})}$  is the hyperfine-splitting-independent detuning of the laser frequency  $\omega$  to the reference frequency of the optical transition  $\omega^{(\text{eg})}$ .

In addition to the coherent mechanisms governed by the Hamiltonians  $H_0$  and  $H_{\text{int}}$ , the atoms experience incoherent dynamics, including level broadening and spin relaxation due to atomic collisions, spontaneous emission of photons, and non-radiative decay (quenching) processes. Due to these incoherent processes, the optical ES are hardly occupied. In this case, the ES degree of freedom and the optical coherences are adiabatically eliminated [9]. Therefore, the evolution of atomic spin is reduced to the master equation in GS Liouville space [23]

$$\frac{d}{dt} |\rho^{(\text{gg})}\rangle = - \left( iH^{(\text{g})\odot} + \mathcal{G}_{\text{rel}}^{(\text{g})} + R_{\text{op}} \mathcal{A}_{\text{op}} \right) |\rho^{(\text{gg})}\rangle, \quad (6)$$

where  $|\rho^{(\text{gg})}\rangle$  is the vectorized GS density matrix, and  $X^{\odot} = X^{\flat} - X^{\sharp}$  is the commutator superoperator with  $X^{\flat}$  and  $X^{\sharp}$  the left- and right-translation superoperators [17], corresponding to the operator  $X$  in Hilbert space. The GS spin relaxation term  $\mathcal{G}_{\text{rel}}^{(\text{g})}$  is

$$\mathcal{G}_{\text{rel}}^{(\text{g})} = \Gamma_{\text{SD}} \mathcal{A}_{\text{SD}} + \Gamma_{\text{ex}} (\mathcal{A}_{\text{SD}} - (\mathbf{S}|\rho) \cdot \mathcal{A}_{\text{SE}}), \quad (7)$$

with the spin-destruction rate  $\Gamma_{\text{SD}}$ , the spin-exchange rate  $\Gamma_{\text{ex}}$ , and the mean electron spin polarization  $(\mathbf{S}|\rho^{(\text{gg})}) = \text{Tr}[\mathbf{S}\rho^{(\text{gg})}]$ . The spin-destruction and spin-exchange superoperators  $\mathcal{A}_{\text{SD}}$  and  $\mathcal{A}_{\text{SE}}$  are

$$\mathcal{A}_{\text{SD}} = \frac{3}{4} - \mathbf{S}^{\flat} \cdot \mathbf{S}^{\sharp}, \quad (8)$$

$$\mathcal{A}_{\text{SE}} = \mathbf{S}^{\flat} + \mathbf{S}^{\sharp} - 2i\mathbf{S}^{\flat} \times \mathbf{S}^{\sharp}, \quad (9)$$

where  $\mathbf{S}$  is the electron spin operator of the alkali-metal atom.

The optical pumping process is described by the third term of the right-hand-side of Eq. (6), where  $R_{\text{op}}$  is the optical pumping rate and  $\mathcal{A}_{\text{op}}$  is the corresponding superoperator. The optical pumping process consists of two parts [9, 17]

$$\mathcal{A}_{\text{op}} = \mathcal{A}_{\text{dp}} - \mathcal{A}_{\text{rp}}, \quad (10)$$

where  $\mathcal{A}_{\text{dp}}$  and  $\mathcal{A}_{\text{rp}}$  represent the depopulation and repopulation processes, respectively. The depopulation term  $\mathcal{A}_{\text{dp}}$  is associated with light absorption and removes population from the GS,

$$R_{\text{op}} \mathcal{A}_{\text{dp}} = i[V^\dagger W]^\odot \equiv i[\delta H^{(\text{g})}]^\odot, \quad (11)$$

where

$$W = V / (\Delta^{(\text{eg})} + i\Gamma_{\text{brd}}). \quad (12)$$

In Eq. (12),  $\Delta^{(\text{eg})} = [\Delta_{\bar{F}\bar{m}_F, Fm_F}]$  is the detuning matrix with elements defined in (5), and the dot-slash product is defined by  $\langle \nu|A|B|\mu\rangle = \langle \nu|A|\mu\rangle / \langle \nu|B|\mu\rangle$  for matrices  $A$  and  $B$  [17]. The repopulation term  $\mathcal{A}_{\text{rp}}$ , describing the optical excitation, spin relaxation, and quenching of the atomic ES and restoring the GS, is shown to be the form [23]

$$\mathcal{A}_{\text{rp}} = \Gamma_{\text{q}} \mathcal{A}_{\text{q}}^{(\text{ge})} \left[ iH^{(\text{e})\odot} + \Gamma_{\text{q}} + \Gamma_{\text{JD}} A_{\text{JD}} \right]^{-1} \mathcal{A}_{\text{p}}^{(\text{eg})}, \quad (13)$$

where  $\mathcal{A}_{\text{q}}^{(\text{ge})}$  is the superoperator of quenching process with corresponding quenching rate  $\Gamma_{\text{q}}$ , and  $\mathcal{A}_{\text{JD}}$  is the superoperator of the spin relaxation process of ES with the damping rate  $\Gamma_{\text{JD}}$ . Analytical expressions of  $\mathcal{A}_{\text{q}}^{(\text{ge})}$  and  $\mathcal{A}_{\text{JD}}$  are obtained by the uncoupled irreducible tensor operators, and can be found in Refs. [13, 23]. In Eq. (13), the superoperator  $\mathcal{A}_{\text{p}}^{(\text{eg})}$  is defined as [17]

$$\mathcal{A}_{\text{p}}^{(\text{eg})} = -V^* \otimes W + W^* \otimes V, \quad (14)$$

which describes the optical excitation of the atoms from the GS to the ES. Here,  $\otimes$  denotes the Kronecker product between operators in Hilbert space.

## B. Optical pumping in quasi-high-pressure regime

### 1. Depopulation

The energy denominator matrices  $\Delta^{(\text{eg})} + i\Gamma_{\text{brd}}$  in Eqns. (11) and (13) play the central rule in describing optical pumping in different buffer-gas regimes. As discussed in Sec. II, in

the HP limit they simply merge into  $\Delta_0 \pm i\Gamma_{\text{brd}}$ . Through this approximation, one can obtain  $\mathcal{A}_{\text{dp}}^{(\text{HP})}$  [17].

$$A_{\text{dp}}^{(\text{HP})} = 1 - \mathbf{s} \cdot (\mathbf{S}^b + \mathbf{S}^a) - i\mathbf{s} \cdot \mathbf{S}^\odot, \quad (15)$$

with  $\mathbf{s} = i\hat{\mathbf{e}} \times \hat{\mathbf{e}}^*$  the mean photon spin. Here, the identity for  $D_1$  line is utilized

$$\hat{\mathbf{e}}^* \cdot d d^\dagger \cdot \hat{\mathbf{e}} = \frac{1}{2} - \mathbf{s} \cdot \mathbf{S}, \quad (16)$$

which expresses how the electric-dipole operator links the GS spin operator.

In the QHP regime of interest, the energy denominators are naturally grouped by  $\Delta_F \pm i\Gamma_{\text{brd}}$ , which characterizes the resolvable  $F = a$  and  $b$  multiplets and their distinct contributions to optical pumping. In this way, elements of  $\delta H^{(\text{g})}$  are simplified as

$$\langle F' m'_F | \delta H | F m_F \rangle = \frac{\langle F' m'_F | \mathcal{V}^\dagger \mathcal{V} | F m_F \rangle}{\Delta_F + i\Gamma_{\text{brd}}}, \quad (17)$$

with  $\Delta_F$  being the reference detuning determined by the  $F$  multiplet for  $F = a$  or  $F = b$

$$\Delta_F = \Delta_0 + \omega_{F,0}^{(\text{g})}. \quad (18)$$

The amplitude of  $\delta H^{(\text{g})}$  is evaluated by  $R_{\text{op}} = \sigma_0 \Phi$ , where  $\sigma_0$  becomes a sum of two Lorentzian line shapes

$$\sigma_0 = A_0 \left( \frac{[a]}{2[I]} \frac{\Gamma_{\text{brd}}}{\Delta_a^2 + \Gamma_{\text{brd}}^2} + \frac{[b]}{2[I]} \frac{\Gamma_{\text{brd}}}{\Delta_b^2 + \Gamma_{\text{brd}}^2} \right). \quad (19)$$

with  $[N] = 2N + 1$  for a quantum number  $N$  and  $A_0$  being the D line constant [9]

$$A_0 = \frac{|\Omega_1|^2}{\Phi} = r_e c f^{(\text{ge})}. \quad (20)$$

Here  $r_e$  is the classical electron radius,  $c$  is the speed of light and  $f^{(\text{ge})}$  the oscillator strength. Using Eqs. (17) and (19), we obtain the imaginary and real part of  $\delta H^{(\text{g})}$  compactly

$$\delta H^{(\text{g})} = R_{\text{op}} \left( \frac{1}{2} - \mathbf{s} \cdot \mathbf{S} \right) (2\mathcal{K}_{\mathcal{H}} - i\mathcal{Q}_{\mathcal{H}}), \quad (21)$$

which both take the form of  $\delta H^{(\text{g})}$  in the HP limit followed by the diagonal matrix  $\mathcal{Q}_{\mathcal{H}}$  and  $\mathcal{K}_{\mathcal{H}}$

$$\mathcal{K}_{\mathcal{H}} = \sum_{F=a,b} \sum_{m_F} K_F |F m_F\rangle \langle F m_F|, \quad (22)$$

$$\mathcal{Q}_{\mathcal{H}} = \sum_{F=a,b} \sum_{m_F} Q_F |F m_F\rangle \langle F m_F|. \quad (23)$$

As shown in Fig. 2, the detuning-dependent factor  $Q_F$  is

$$Q_F = \frac{2[I](\Delta_F^2 + \Gamma_{\text{brd}}^2)^{-1}}{[a](\Delta_a^2 + \Gamma_{\text{brd}}^2)^{-1} + [b](\Delta_b^2 + \Gamma_{\text{brd}}^2)^{-1}} \quad (24)$$

and  $K_F = Q_F \Delta_F / \Gamma_{\text{brd}}$ . The form in Eq. (21) captures the contribution of each GS hyperfine multiplet to light absorption

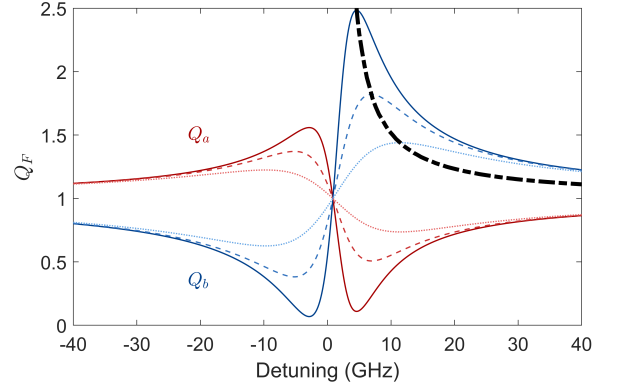


FIG. 2. Detuning-dependent factor  $Q_F$  for  $F = a$  and  $F = b$  [see Eq. (24)]. Solid, dashed, and dotted curves represent  $\Gamma_{\text{brd}} = 3, 10$  and  $20$  GHz. They converge to a common intersection at  $\Delta_a = \Delta_b$ , yielding  $Q_a = Q_b = 1$ . The thick black dashed curve shows the maximum attainable  $Q_b$  for varying  $\Gamma_{\text{brd}}$ .

and optical shift, since the factor  $(\Delta_F^2 + \Gamma_{\text{brd}}^2)^{-1}$  weights the spectral response of the  $F$  multiplet.

Based on the QHP-specific corrections of  $\delta H^{(\text{g})}$  in Eq. (17), it is proved that in Liouville space,  $\mathcal{A}_{\text{dp}}$  similarly takes a form that links to the HP counterpart  $\mathcal{A}_{\text{dp}}^{(\text{HP})}$

$$\text{Re}[\mathcal{A}_{\text{dp}}]_{m,n} = \text{Re}[\mathcal{A}_{\text{dp}}^{(\text{HP})}]_{m,n} \mathcal{Q}_{\mathcal{L}}^{(n)}, \quad (25)$$

$$\text{Im}[\mathcal{A}_{\text{dp}}]_{m,n} = \text{Im}[\mathcal{A}_{\text{dp}}^{(\text{HP})}]_{m,n} \mathcal{K}_{\mathcal{L}}^{(n)}, \quad (26)$$

where  $[\mathcal{X}]_{m,n}$  labels the matrix block of a superoperator  $\mathcal{X}$ , responsible for coupling  $n$ th-order to  $m$ th-order Zeeman coherences. The block decomposition in Liouville space serves as an efficient method for treating master equations, detailed in the Appendix. A. Here in Eqs. (25) and (26), the QHP-specific matrices  $\mathcal{Q}_{\mathcal{L}}^{(n)}$  and  $\mathcal{K}_{\mathcal{L}}^{(n)}$  are

$$\mathcal{Q}_{\mathcal{L}}^{(k)} = \sum_F \sum_{m_F} Q_F \mathcal{P}_F^{(k)}, \quad (27)$$

$$\mathcal{K}_{\mathcal{L}}^{(k)} = \sum_F \sum_{m_F} K_F \mathcal{P}_F^{(k)}. \quad (28)$$

This result can be mathematically viewed as a linear column transformation acting on the HP superoperator in Zeeman subspace. Together with the next section, we present that  $A_{\text{dp}}$  and  $A_{\text{rp}}$  both adopt the analogous form. The detailed proofs are provided in the Appendix. B.

## 2. Repopulation

The repopulation term in Eq. (13) represents the generation and relaxation of the atomic ES spin during the optical pumping process. In the same way of dealing with  $\mathcal{A}_{\text{dp}}$ , we primarily simplify  $\mathcal{A}_{\text{p}}^{(\text{eg})}$  in Eq. (13) as

$$[\mathcal{A}_{\text{p}}^{(\text{eg})}]_{\bar{m},n} = [2(\hat{\mathbf{e}}^* \cdot \Delta^{\text{T}}) \otimes (\Delta^\dagger \cdot \hat{\mathbf{e}})]_{\bar{m},n} \mathcal{Q}_{\mathcal{L}}^{(n)}, \quad (29)$$

Here  $\bar{m}$  denotes the ES  $\bar{m}$ th-order Zeeman coherence subspace and its projection operator remains the same with Eq. (A1) for  $D_1$  line. This result physically means that detunings  $\Delta_F$  for  $F = a, b$  contribute differently to the excitation transfer.

For ES relaxation and ES-GS transition that occurs in Eq. (13), Appelt *et al.* show that dominant mechanisms are typically J-damping collision and quenching [23]. Thus  $\mathcal{A}_{\text{rp}}$  can be expanded in power series of  $H^{(e)\odot}$ , retaining only the leading term

$$\mathcal{A}_{\text{rp}} \approx \mathcal{A}_{\text{rp}}^{(0)} = \left(1 - \mathcal{A}_{\text{q}}^{(\text{ge})}\right) \left(1 - \mathcal{A}_{\text{JD}}\right) \mathcal{A}_{\text{p}}^{(\text{eg})}, \quad (30)$$

while the first-order perturbation from  $H^{(e)\odot}$  is given by

$$\mathcal{A}_{\text{rp}}^{(1)} = \left(1 - \mathcal{A}_{\text{q}}^{(\text{ge})}\right) \frac{iH^{(\text{ee})\odot}}{\Gamma_{\text{q}}} \left(1 - \mathcal{A}_{\text{JD}}\right) \mathcal{A}_{\text{p}}^{(\text{eg})}. \quad (31)$$

Under lower pressure (e.g., 0.01 ~ 0.1 amg for  $\text{N}_2$ ), a systematic investigation in [13] offers a scale of correction from  $H^{(e)\odot}$ . For theoretical simplicity, we still adopt the approximation of Eq. (30) in the following analysis.

As already researched [17, 23], J-Damping collision and quenching fully transfer nuclear polarization with no transfer of electronic polarization. Furthermore, any mechanism originating from the electric-dipole interaction only manipulate the electronic part of a density matrix, and assure nuclear spin invariant, due to its short interaction timescale. So superoperators  $\mathcal{A}_{\text{dp}}$  and  $\mathcal{A}_{\text{rp}}$  share a common nuclear part

$$\mathcal{A}_{\text{rp}} = \left(1 - \mathcal{A}_{\text{q}}^{(\text{ge})}\right) \mathcal{A}_{\text{p}}^{(\text{eg})} = \left(1 - \mathcal{A}_{\text{SD}}\right) \mathcal{A}_{\text{dp}}, \quad (32)$$

Through Eqs. (10), (25), (26), and (32), the full optical pumping superoperator  $\mathcal{A}_{\text{op}}$  in the Zeeman subspace is

$$\text{Re}[\mathcal{A}_{\text{op}}]_{m,n} = \text{Re}[\mathcal{A}_{\text{op}}^{(\text{HP})}]_{m,n} \mathcal{Q}_{\mathcal{L}}^{(n)}, \quad (33)$$

$$\text{Im}[\mathcal{A}_{\text{op}}]_{m,n} = \text{Im}[\mathcal{A}_{\text{op}}^{(\text{HP})}]_{m,n} \mathcal{K}_{\mathcal{L}}^{(n)}, \quad (34)$$

where detuning-independent  $\mathcal{A}_{\text{op}}^{(\text{HP})}$  is optical pumping superoperator in the HP limit, and its real and imaginary parts are

$$\text{Re}[\mathcal{A}_{\text{op}}^{(\text{HP})}]_{m,n} = [\mathcal{A}_{\text{SD}}]_{m,n} - \frac{\mathbf{s}}{2} \cdot [\mathcal{A}_{\text{SE}}]_{m,n}, \quad (35)$$

$$\text{Im}[\mathcal{A}_{\text{op}}^{(\text{HP})}]_{m,n} = -i[\mathbf{s} \cdot \mathbf{S}^{\odot}]_{m,n}. \quad (36)$$

respectively, leading to incoherent evolution and frequency shift. In Eqs. (33) and (34), diagonal  $\mathcal{Q}_{\mathcal{L}}^{(n)}$  and  $\mathcal{K}_{\mathcal{L}}^{(n)}$  carry all dependence of hyperfine-resolved detuning  $\Delta_F$ . Matrix structure and detuning dependence of  $\text{Re}[\mathcal{A}_{\text{op}}]_{m,n}$  are illustrated in Fig. 3. As for  $D_2$  line, we should make the replacement  $\mathbf{s} \rightarrow -\mathbf{s}/2$  [9].

Thus, in the QHP regime, we derive a compact form of  $\mathcal{A}_{\text{op}}$  in Zeeman in Eq. (6), with other relaxation superoperators formally unchanged.

### C. Evolution in longitudinal pumping

Longitudinal pumping is an usual configuration in vapor-cell systems, where the average photon spin  $\mathbf{s}$  and the static

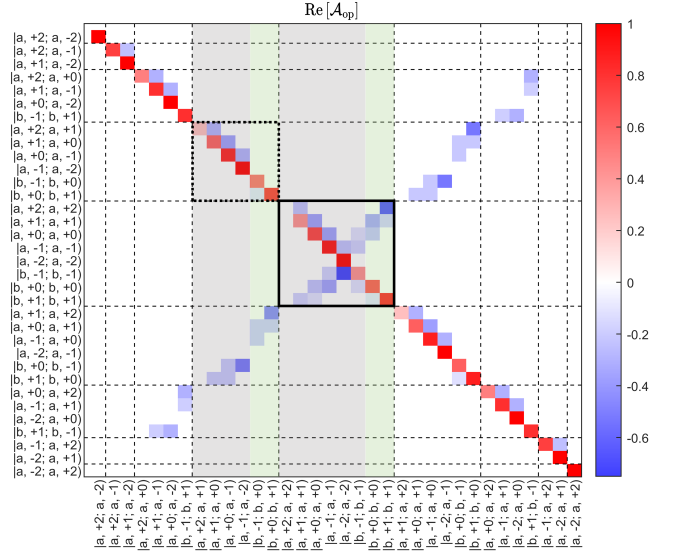


FIG. 3. Heat-map plot of the superoperator  $\text{Re}[\mathcal{A}_{\text{op}}]$  with nuclear spin  $I = 3/2$  and  $\mathbf{s} = \hat{z}$ . The underlying matrix elements are arranged with basis labeled by  $|F, m_F; F, m'_F\rangle$  and presented in the HP limit. They are separated by dashed lines into  $m$ th- to  $n$ th- order Zeeman coherence blocks (see Appendix. A). The block marked by the solid lines is  $[\mathcal{A}_{\text{op}}]_{0,0}$  which governs population pumping, while  $\text{Re}[\mathcal{A}_{\text{op}}]_{1,1}$  marked by the dotted lines contributes to evolution of the 1st-order Zeeman coherence. The vertical gray and green bands encode the detuning-dependent  $Q_F$  for  $F = a, b$ , acting in the QHP regime. Other blocks follow the same way.

magnetic field  $\mathbf{B}$  are both along the quantization axis. So we set  $\mathbf{s} = s\hat{z}$  and  $\mathbf{B} = B\hat{z}$  for simplicity. For atomic magnetometers, in which a weak transverse radio-frequency (RF) field is applied, evolution and steady state of  $|\rho^{(\text{eg})}\rangle$  can be reduced to that in subspaces of the population and 1st-order Zeeman coherences. Accordingly, we concentrate on observables that manifest this steady-state behavior in experiments, including the photon absorption cross section, spin polarization, and magnetic resonance linewidth.

#### 1. Light absorption of atoms

Light absorption of atoms initially enables optical pumping, quantified by the measurable photon cross section  $\sigma$ . It is generally given by an induced electric dipole moment ( $\mathbf{d}$ ) that oscillates with the light frequency  $\omega$  and dissipates the light intensity [17]

$$\sigma_{\text{tot}} = \frac{1}{\Phi_{\omega^{(\text{eg})}}} \left( \Omega_{\text{I}}^* \hat{\mathbf{e}}^* \cdot \frac{d}{dt} \langle \mathbf{d} \rangle + \text{c.c.} \right). \quad (37)$$

In buffer-gas cells where the ES is well adiabatically eliminated, the GS population  $|\rho_0\rangle = \mathcal{P}_{\text{Z}}^{(0)} |\rho^{(\text{eg})}\rangle$  that satisfies normalization  $(1^{|\text{g}\rangle} | \rho_0) = 1$  can sufficiently determine  $\sigma$

$$\sigma = -\frac{2}{\Phi} \left( \text{Im} [\delta H^{|\text{g}\rangle}] | \rho_0 \right). \quad (38)$$

Using  $\delta H^{(g)}$  given in Eq. (21), we have

$$\sigma = \sigma_0(1^{(g)}|Q_{\mathcal{H}}|\rho_0) - 2s\sigma_0(S_z|Q_{\mathcal{H}}|\rho_0). \quad (39)$$

Here  $\sigma_0$  can be obtained as Eq. (19) by substituting  $|\rho_0\rangle = |1^{(g)}\rangle/(2|I\rangle)$  in Eq. (38). For arbitrary  $|\rho_0\rangle$ , Eq. (39) naturally separates  $\sigma$  into two contributions. The first term represents absorption of the unpolarized hyperfine multiplets  $F = a, b$ , weighted with the factors  $Q_F$  contained in  $Q_{\mathcal{H}}$ . The second term accounts for absorption correction of polarized atoms. In particular, population that accumulates in the stretched states  $|F = a, m_F = a\rangle$  weakens the absorption of circularly polarized photons. With  $s = \pm 1, 0$  and the corresponding steady state of  $|\rho_0\rangle$  in the section below,  $\sigma_{\text{lin}}$  and  $\sigma_{\text{cir}}$ , the cross section of circular and linear polarized photons, will be obtained, respectively. They are both expressed as linear combinations of the components associated with the two multiplets

$$\sigma = C_a \frac{A_0\Gamma_{\text{brd}}}{\Delta_a^2 + \Gamma_{\text{brd}}^2} + C_b \frac{A_0\Gamma_{\text{brd}}}{\Delta_b^2 + \Gamma_{\text{brd}}^2}, \quad (40)$$

where the coefficient  $C_F$  for  $F = a, b$  is

$$C_F = p_F - 2s\langle S_z \rangle_F, \quad (41)$$

with  $p_F$  being total population of hyperfine F-multiplet and  $\langle S_z \rangle_F$  describing contribution of the F-multiplet to  $\langle S_z \rangle$

$$p_F = \sum_{m_F} \langle Fm_F; Fm_F | \rho_0 \rangle, \quad (42)$$

$$\langle S_z \rangle_F = \sum_{m_F} \langle S_z | Fm_F; Fm_F \rangle \langle Fm_F; Fm_F | \rho_0 \rangle. \quad (43)$$

This means that calculations of  $\sigma_{\text{lin}}$  and  $\sigma_{\text{cir}}$  generally require a definite form of  $|\rho_0\rangle$ , which is discussed below.

## 2. Steady state population

In the presence of the light absorption and other relaxation mechanisms in Eq. (6), the population dynamics are governed by

$$\frac{d|\rho_0\rangle}{dt} = -\mathcal{G}_{\text{pop}}|\rho_0\rangle. \quad (44)$$

with the kernel  $\mathcal{G}_{\text{pop}}$

$$\begin{aligned} \mathcal{G}_{\text{pop}} = & \Gamma_{\text{SD}} [A_{\text{SD}}]_{0,0} \\ & + R_{\text{op}} \left( [A_{\text{SD}}]_{0,0} - \frac{s}{2} [A_{\text{SE}}^{(z)}]_{0,0} \right) Q_{\mathcal{L}}^{(0)} \\ & + \Gamma_{\text{ex}} \left( [A_{\text{SD}}]_{0,0} - \langle S_z | \rho_0 \rangle [A_{\text{SE}}^{(z)}]_{0,0} \right), \end{aligned} \quad (45)$$

where the average electron spin  $\langle S_z | \rho_0 \rangle = \text{Tr} [S_z \rho_0]$ . We explore this equation as a Markov chain [24] of classical probability, and particularly emphasis on its unique steady state  $|\rho_{\text{st}}\rangle = |\rho_0(t \rightarrow +\infty)\rangle$ , which is most relevant in practice. Here,  $|\rho_{\text{st}}\rangle$  is given by the null space of  $\mathcal{G}_{\text{pop}}$ . We found that the un-stretched state with  $m \in [-b, b]$  generally satisfies

$$\frac{\langle am; am | \rho_{\text{st}} \rangle}{\langle bm; bm | \rho_{\text{st}} \rangle} = \frac{\Gamma_{\text{ex}} + \Gamma_{\text{SD}} + R_{\text{op}} Q_b}{\Gamma_{\text{ex}} + \Gamma_{\text{SD}} + R_{\text{op}} Q_a}. \quad (46)$$

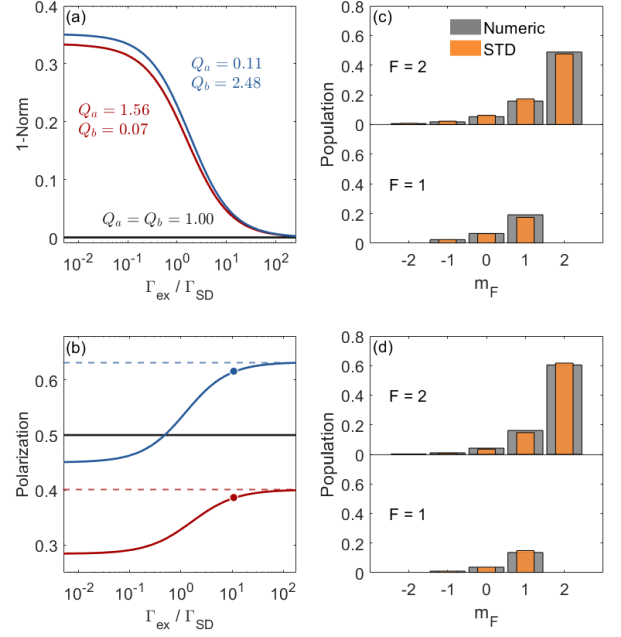


FIG. 4. (a) The 1-norm distance between the steady-state population and the STD with the same polarization. The curves correspond to different detuning-dependent factors  $Q_F$  for  $F = a, b$ . (b) Electron-spin polarization  $P$  versus  $\Gamma_{\text{ex}}/\Gamma_{\text{SD}}$ , with color coding identical to (a) setting. (c) Steady-state population obtained with  $\Gamma_{\text{ex}}/\Gamma_{\text{SD}} = 10$ , corresponding to the point marked on the red curve in (b). STD with the same polarization is shown and compared. (d) Same as (c) but corresponding to the blue marked point in (b). All results are computed for  $I = 3/2$  and  $s = 1$ , fixing  $R_{\text{op}}/\Gamma_{\text{SD}} = 1$ .

This directly illustrates the effective pumping effect between the  $a$  and  $b$  multiplets, which vanishes in the HP limit. We next turn to specific cases corresponding to different mean photon spin  $s$ .

For circularly polarized photons such as  $s = 1$ , the steady state no longer satisfies the detailed balance, namely spin temperature distribution (STD) [20, 23], which can be obtained only with  $Q_F = 1$ . The numerical solution in Fig. 4(a) describes its deviation from STD. Also in contrast to the HP limit, we further found that the electron spin polarization  $P$ , defined as

$$P \equiv 2\langle S_z \rangle = 2\langle S_z | \rho_{\text{st}} \rangle, \quad (47)$$

becomes dependent on the spin exchange rate  $\Gamma_{\text{ex}}$ , as shown in Fig. 4(b). This is because when the rapidly oscillating hyperfine coherence decays, spin exchange collision no longer conserves spin for states beyond STD.

However, with typical parameters, especially temperature (80 °C or higher) in experiments, a sufficiently large  $\Gamma_{\text{ex}}$  [10] can ensure that STD is still a good approximation. As an example, Fig. 4(c) and Fig. 4(d) display  $|\rho_{\text{st}}\rangle$  for  $\Gamma_{\text{ex}}/\Gamma_{\text{SD}} = 10$ , where the deviation from STD is small enough. At a temperature higher than 60 °C, the deviation will be less than this. Therefore, while remaining within the QHP regime, we still adopt the STD limit, in which the steady state population is

assumed to be  $|\rho_{\text{st}}^{(\text{STD})}\rangle$  determined by  $P$

$$(Fm_F; Fm_F | \rho_{\text{st}}^{(\text{STD})} ) = \frac{P(1+P)^{\frac{|l|}{2+m_F}}(1-P)^{\frac{|l|}{2-m_F}}}{(1+P)^{|l|} - (1-P)^{|l|}}. \quad (48)$$

In Sec. IV, we will give  $p_F$ ,  $\langle S_z \rangle_F$  and  $C_F$  in Eqs. (41), (42) and (43) in the STD limit, which enables renewed absorption cross section  $\sigma$  and polarization  $P$ .

### 3. Weak driving magnetic resonance

A practical application of longitudinal pumping is atomic magnetometers based on magnetic resonance, which lies in the population imbalance among  $m_F$  sublevels created by circularly polarized photons, with  $s = 1$  for simplicity. This essentially enables the transverse RF field to drive Zeeman coherences [23]. In our previous work for unresolved Zeeman resonance [19], we considered an radio-frequency (RF) driving field along the  $\hat{x}$  axis

$$H_{\text{drv}} = \Omega_R S_x \cos(\omega_{\text{rf}} t) \quad (49)$$

whose oscillation frequency  $\omega_{\text{rf}}$  far exceeds the Larmor frequency  $\Omega_L$ , i.e., the linear Zeeman splitting. We assumed that the Rabi frequency  $\Omega_R$  is weak enough to keep  $|\rho_{\text{st}}\rangle$  unchanged and only 1st-order Zeeman coherence  $|\tilde{\rho}_1\rangle$  generated for steady state. Therefore, a framework in the rotating RF frame is established for  $|\tilde{\rho}_1\rangle$

$$|\tilde{\rho}_1\rangle = -\frac{i\Omega_R}{2} \mathcal{G}_{\text{WDA}}^{-1} [S_x^\odot]_{1,0} |\rho_{\text{st}}\rangle, \quad (50)$$

where  $[S_x^\odot]_{1,0}$  generates  $|\tilde{\rho}_1\rangle$  from polarized atomic population  $|\rho_0\rangle$ , and  $\mathcal{G}_{\text{WDA}}$  is a total relaxation superoperator of  $|\tilde{\rho}_1\rangle$ . Following this framework, the optical pumping contribution should be replaced by  $[A_{\text{op}}]_{1,1}$ , whose real part related to decoherence is shown in Fig. 3, and the imaginary part leading to frequency shifts is

$$\text{Im} [A_{\text{op}}]_{1,1} = \frac{\Delta_a Q_a}{[I]\Gamma_{\text{brd}}} \mathcal{P}_a^{(1)} + \frac{\Delta_b Q_b}{[I]\Gamma_{\text{brd}}} \mathcal{P}_b^{(1)}. \quad (51)$$

Meanwhile, all other relaxation terms in  $\mathcal{G}_{\text{WDA}}$  remain formally unchanged.

In typical magnetometers, transverse spin component is measured via the Faraday rotation effect [3, 25]. Accordingly, the unresolved Zeeman resonance can be well described by a complex response amplitude [19]

$$S = (S_x |\tilde{\rho}_1\rangle) \approx \frac{\Omega_R}{2} \frac{W}{\Delta_{\text{rf}} + i\Gamma_2} \quad (52)$$

where  $\Delta_{\text{rf}} = \omega_{\text{rf}} - \Omega_L - \delta\Omega_L$  is the effective RF detuning, with  $\delta\Omega_L$  being the optical shift, i.e. light-induced AC-Stark shift to  $\Omega_L$ . The linewidth  $\Gamma_2$  is the lowest eigenvalue of  $\mathcal{G}_{\text{WDA}}$  with its weight factor  $W$ , which strongly dominates the exact  $S$ . This eigenvalue exists in the a-subspace, which renders  $\delta\Omega_L$  determined by the corresponding frequency shift in Eq. (51)

$$\delta\Omega_L \approx \frac{1}{[I]} \frac{\Phi A_0 \Delta_a}{\Delta_a^2 + \Gamma_{\text{brd}}^2}. \quad (53)$$

As observable signals, the in-phase and out-of-phase quadratures are

$$X = \text{Re}[S] = \frac{\Omega_R}{2} \frac{W \Delta_{\text{rf}}}{\Delta_{\text{rf}}^2 + \Gamma_2^2}, \quad (54)$$

$$Y = -\text{Im}[S] = \frac{\Omega_R}{2} \frac{W \Gamma_2}{\Delta_{\text{rf}}^2 + \Gamma_2^2}. \quad (55)$$

The amplitude  $Y_{\text{max}} = \Omega_R W / \Gamma_2$  with  $\Delta_{\text{rf}} = 0$  describes the maximum response of atomic magnetometers.

In Sec. IV C, observables associated with atomic magnetometer performance,  $\Gamma_2$  and  $Y_{\text{max}}$ , will be investigated in detail to demonstrate how the magnetic resonance is enhanced at specific laser detuning. The framework in the QHP regime can be straightforwardly extended to the study of resolved Zeeman resonance [1, 23, 26], with only modifications accounting for the contribution of optical pumping with the  $F = a, b$  multiplets resolved.

## IV. RESULTS AND DISCUSSION

### A. Absorption cross section

For optically pumped atoms in the QHP regime, we utilize the description of light absorption in Sec. III C 1 and calculate  $\sigma_{\text{lin}}$  and  $\sigma_{\text{cir}}$ .

For linearly polarized pumping with  $s = 0$ , the atomic spin cannot be polarized and Eq. (44) exactly result in detailed balance [24]. Thus, we can analytically get  $|\rho_{\text{st}}\rangle$  by Eq. (46).

$$|\rho_{\text{st}}^{(s=0)}\rangle = \frac{1}{N_0} \sum_F \sum_{m_F} \left( 1 + \frac{R_{\text{op}} Q_{F'}}{\Gamma_{\text{SD}} + \Gamma_{\text{ex}}} \right) |Fm_F; Fm_F\rangle, \quad (56)$$

with  $F' \neq F$  denoting the other hyperfine multiplet distinct from  $F$ , and  $N_0 = 2[I] + ([a]Q_b + [b]Q_a)R_{\text{op}}$  being the normalization factor. Due to unresolved  $m_F$  sublevels within the  $F$  multiplet, an effective three-level model featured in the QHP regime naturally emerges—comprising  $F = a$  and  $F = b$  together with the ES—capturing the optical excitation and relaxation pathways. For the steady state given by Eq. (56),  $R_{\text{op}} Q_{F'}$  plays the role of an effective transfer between the GS hyperfine multiplets, while  $\Gamma_{\text{ex}} + \Gamma_{\text{SD}}$  characterizes the relaxation-induced population exchange between the two hyperfine multiplets, leading to a distribution governed by their degeneracies. Populations in the hyperfine multiplets  $F = a$  and  $F = b$  contribute to the light absorption differently, and  $\sigma_{\text{lin}}$  can be expressed as

$$\sigma_{\text{lin}} = C_a^{(\text{lin})} \frac{A_0 \Gamma_{\text{brd}}}{\Delta_a^2 + \Gamma_{\text{brd}}^2} + C_b^{(\text{lin})} \frac{A_0 \Gamma_{\text{brd}}}{\Delta_b^2 + \Gamma_{\text{brd}}^2}, \quad (57)$$

where the coefficients  $C_a^{(\text{lin})}$  and  $C_b^{(\text{lin})}$  take the same form [ $F' \neq F$  same as in Eq.(56)]

$$C_F^{(\text{lin})} = \frac{\Gamma_{\text{SD}} + \Gamma_{\text{ex}} + R_{\text{op}} Q_{F'}}{2[I](\Gamma_{\text{SD}} + \Gamma_{\text{ex}}) + ([a]Q_b + [b]Q_a)R_{\text{op}}}, \quad (58)$$

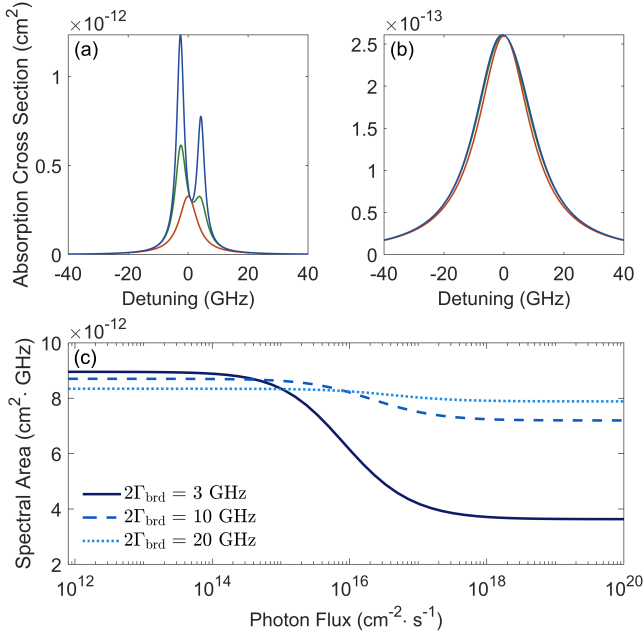


FIG. 5. (a) Absorption cross section  $\sigma_{\text{lin}}$  ( $s = 0$ ) versus laser detuning  $\Delta_0$  with  $\Gamma_{\text{brd}} = 3$  GHz. The blue, green, and red curves correspond to  $\Phi = 10^{12}$ ,  $10^{16}$ , and  $10^{20}$   $\text{cm}^{-2} \text{s}^{-1}$ , respectively. (b) Same as (a), but for a typical HP case,  $2\Gamma_{\text{brd}} = 20$  GHz. (c) Integrated spectral area obtained by  $\int \sigma_{\text{lin}} d\Delta_0$ , plotted for different  $\Gamma_{\text{brd}}$ . Relaxation rates,  $\Gamma_{\text{ex}}$  and  $\Gamma_{\text{SD}}$ , correspond to  $^{87}\text{Rb}$  with  $\text{N}_2$  buffer gas at  $100^\circ\text{C}$ .

The results of  $\sigma_{\text{lin}}$  are shown in Fig. 5, where a notable feature emerges for finite  $\Phi$ . In the QHP regime, the resonance peaks of  $\sigma_{\text{lin}}$  for pumped atoms become significantly suppressed and unresolved. This behavior is evident in Fig. 5(a), while it is absent in the HP limit as shown in Fig. 5(b). A mechanism directly revealed by this is an effective pumping effect between  $F = a, b$  multiplets. That is, when  $\Delta_F = 0$ , population in the  $F$  multiplet is more efficiently pumped into the other.

As another observable feature, in contrast to  $\sigma_0$  in weak-pumping limit  $\Phi \rightarrow 0$ , we find that  $\sigma_{\text{lin}}$  in strong pumping limit  $R_{\text{op}} \gg \Gamma_{\text{SD}} + \Gamma_{\text{ex}}$  (but assure no population trapped in the ES) does not vanish but instead asymptotically approaches a finite value

$$\sigma_{\text{lin}}(R_{\text{op}} \gg \Gamma_{\text{SD}} + \Gamma_{\text{ex}}) = \frac{A_0 \Gamma_{\text{brd}}}{(\Delta_0 - \omega_{\text{eff}})^2 + \Gamma_{\text{eff}}^2}, \quad (59)$$

which takes a Lorentzian form with  $\omega_{\text{eff}}$  and  $\Gamma_{\text{eff}}$  being the effective resonance frequency and linewidth,

$$\omega_{\text{eff}} = \frac{[a]}{2[I]} \omega_{a,0}^{(g)} + \frac{[b]}{2[I]} \omega_{b,0}^{(g)}, \quad (60)$$

$$\Gamma_{\text{eff}} = \Gamma_{\text{brd}}^2 + \frac{[a][b]}{2[I]} (\omega_{a,0}^{(g)} + \omega_{b,0}^{(g)})^2. \quad (61)$$

This behavior accounts for the convergence of the spectral area shown in Fig. 5(c), a characteristic that enables experimental reconstruction of the atomic state from the observed absorption spectrum.

Furthermore, for the circularly polarized photon absorption cross section  $\sigma_{\text{cir}}$ , we adopt the STD limit mentioned in

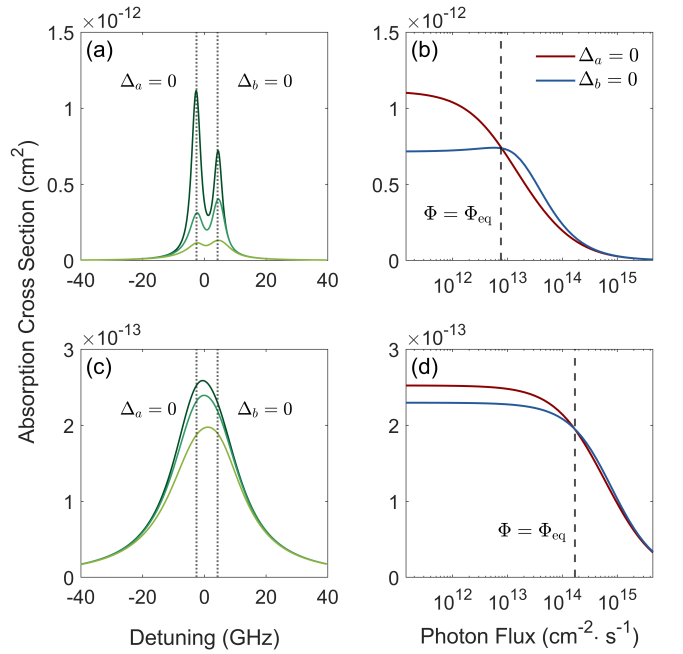


FIG. 6. (a) Absorption cross section  $\sigma_{\text{cir}}$  of with  $s = 1$  and  $2\Gamma_{\text{brd}} = 3$  GHz. Three green solid curves, rendered from dark to light, correspond to photon flux  $\Phi = 0$ ,  $5 \times 10^{13}$ , and  $2 \times 10^{14}$   $\text{cm}^{-2} \text{s}^{-1}$ , respectively. Dotted lines indicate the two characteristic laser detunings. (b)  $\sigma_{\text{cir}}$  as a function of  $\Phi$  at  $\Delta_a = 0$  and  $\Delta_b = 0$ . The intersection point of them  $\sigma_{\text{cir}}(\Delta_a = 0) = \sigma_{\text{cir}}(\Delta_b = 0)$  occurs with  $\Phi_{\text{eq}} = 7.5 \times 10^{13}$   $\text{cm}^{-2} \text{s}^{-1}$  where the polarization is about  $P = 0.2$ . (c–d) The same conditions as in (a–b) are repeated for a larger collisional broadening  $2\Gamma_{\text{brd}} = 20$  GHz, representative of the HP limit. Relaxation rates,  $\Gamma_{\text{ex}}$  and  $\Gamma_{\text{SD}}$ , correspond to  $^{87}\text{Rb}$  with  $\text{N}_2$  buffer gas at  $100^\circ\text{C}$ .

Sec. III C 2, and are able to formally write  $\sigma_{\text{cir}}$  as

$$\sigma_{\text{cir}} = C_a^{(\text{cir})} \frac{A_0 \Gamma_{\text{brd}}}{\Delta_a^2 + \Gamma_{\text{brd}}^2} + C_b^{(\text{cir})} \frac{A_0 \Gamma_{\text{brd}}}{\Delta_b^2 + \Gamma_{\text{brd}}^2}, \quad (62)$$

with  $C_F^{(\text{cir})} = p_F(I, P) - 2s \langle S_z \rangle_F(I, P)$  for  $F = a$  and  $b$ , being a function of the nuclear spin  $I$  and the polarization  $P$ . Using

TABLE I. Expressions for  $p_F(I, P)$  and  $\langle S_z \rangle_F(I, P)$  defined by Eqs. (42) and (43), with  $p_b = 1 - p_a$  and  $\langle S_z \rangle_b = P/2 - \langle S_z \rangle_a$ . These results are derived in the STD limit and used in Eqs. (69) and (62).

$I$	$p_a(I, P)$	$\langle S_z \rangle_a(I, P)$
$\frac{1}{2}$	$\frac{3}{4} + \frac{P^2}{4}$	$\frac{P}{2}$
1	$\frac{2}{3} + \frac{4P^2}{3(3+P^2)}$	$\frac{5P+P^3}{3(3+P^2)}$
$\frac{3}{2}$	$\frac{5}{8} + \frac{5P^2+P^4}{8(1+P^2)}$	$\frac{5P+3P^3}{8(1+P^2)}$
2	$\frac{3}{5} + \frac{4(5P^2+3P^4)}{5(5+10P^2+P^4)}$	$\frac{3P+10P^3+3P^5}{2(5+10P^2+P^4)}$
$\frac{5}{2}$	$\frac{7}{12} + \frac{35P^2+42P^4+3P^6}{12(3+10P^2+3P^4)}$	$\frac{7P+14P^3+3P^5}{3(3+10P^2+3P^4)}$

Eq. (48), expressions of  $p_F(I, P)$  and  $\langle S_z \rangle_F(I, P)$  are both derived and displayed in Table I. For  $I = 3/2$ , as an example, the coefficients in Eq. (62) are

$$C_{a=2}^{(\text{cir})} = \frac{5}{8} - \frac{10P - 5P^2 + 6P^3 - P^4}{8(1 + P^2)}, \quad (63)$$

$$C_{b=1}^{(\text{cir})} = \frac{3}{8} + \frac{2P - 5P^2 - 2P^3 - P^4}{8(1 + P^2)}, \quad (64)$$

Typical results of  $\sigma_{\text{cir}}$  obtained by Eq. (40) are shown in Fig. 6(a) to illustrate how polarized atoms respond to pumping light with different detunings.

To clarify the optimal conditions for optical pumping efficiency, we focus on the relative magnitude of the cross sections at optical resonance,  $\sigma_{\text{cir}}(\Delta_a = 0)$  and  $\sigma_{\text{cir}}(\Delta_b = 0)$ . It is noted that a critical point arises when the two cross sections become exactly equal, which occurs at the photon flux  $\Phi = \Phi_{\text{eq}}$ , as shown in Fig. 6(b). For  $\Phi$  larger than  $\Phi_{\text{eq}}$ , atoms always exhibit stronger absorption of photons with  $\Delta_b = 0$ , and consequently attain a higher polarization  $P$  (as seen in Fig. 7), with the opposite behavior holding for  $\Phi < \Phi_{\text{eq}}$ . This can be understood via how differently polarized atoms respond to the pumping mechanism. For low polarization, the higher degeneracy of the  $a$  multiplet leads to a stronger response to pumping light with  $\Delta_a = 0$ . As polarization builds up, the population is gradually transferred to the stretched dark state  $|F = a, m_F = a\rangle$ , while the remaining population, especially in the  $b$  multiplet which contains opposite polarization induced by spin exchange, still absorbs photons. This renders resonant pumping at  $\Delta_b = 0$  favorable for further polarization, until atoms are almost fully polarized and consequently weaken  $\sigma_{\text{cir}}$  to zero. These different response behaviors can also be explained by  $\text{Im}[\delta H^{(\text{S})}]$  in Eq. (21), whose diagonal elements directly reflect the absorption strength of the corresponding states.

By contrast, in the HP limit, all the cross sections mentioned above collapse to

$$\sigma^{(\text{HP})} = \frac{A_0 \Gamma_{\text{brd}}}{\Delta_0^2 + \Gamma_{\text{brd}}^2} (1 - sP), \quad (65)$$

which apparently takes a simple form but loses validity in the QHP regime.

## B. Electron spin polarization

Motivated by applications in atomic magnetometers, we primarily study the polarization  $P$  in the QHP regime. We execute  $(F_z| = (I_z| + (S_z|$  to both side of Eq. (44) and get an equation of the average total angular momentum  $\langle F_z \rangle$

$$\frac{d\langle F_z \rangle}{dt} = R_{\text{op}} \sum_F Q_F \left( \frac{s}{2} p_F - \langle S_z \rangle_F \right) - \Gamma_{\text{SD}} \langle S_z \rangle, \quad (66)$$

Here, we utilized the identities in the population subspace

$$(F_z| [A_{\text{SD}}]_{0,0} = (S_z|, \quad (67)$$

$$(F_z| [A_{\text{SE}}^{(z)}]_{0,0} = (I^{(\text{S})}|, \quad (68)$$

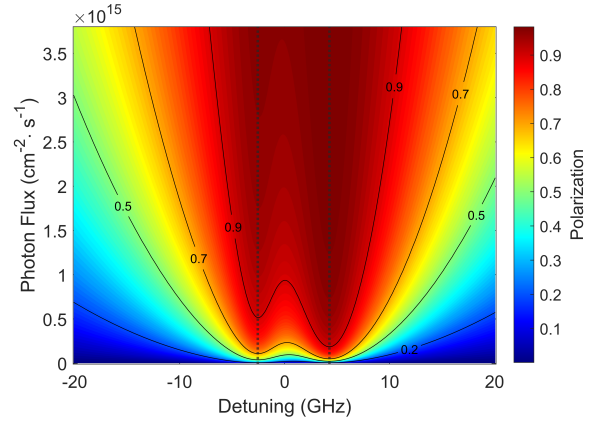


FIG. 7. Two-dimensional color map of the electron spin polarization  $P$  versus  $\Delta_0$  and  $\Phi$ . The vertical dotted lines indicate  $\Delta_a = 0$  and  $\Delta_b = 0$ . The result is obtained by Eq. (69) and well agree with that in the STD limit. Contour lines of  $P$  are overlaid for clarity. All additional atomic and optical parameters are identical to those used in Fig. 6.

which physically means that the S-damping collision conserves the nuclear spin momentum, while the spin exchange conserves the total angular momentum (instead of  $\langle S_z \rangle$ , as presented in Sec. III C 2). Thus, the nonlinear term in Eq. (45) vanishes for  $\langle F_z \rangle$  evolution.

Focusing on the steady state, we set  $d\langle F_z \rangle/dt = 0$  and get the polarization

$$P = \frac{sR_{\text{op}}(Q_a P_a + Q_b P_b)}{R_{\text{op}}(\langle S_z \rangle_a Q_a + \langle S_z \rangle_b Q_b) + \Gamma_{\text{SD}}}, \quad (69)$$

which significantly differs from that in the HP limit ( $Q_F \rightarrow 1$ )

$$P^{(\text{HP})} = \frac{sR_{\text{op}}}{R_{\text{op}} + \Gamma_{\text{SD}}} \quad (70)$$

and depend on the atomic state in general. For simplicity and physical relevance, we still consider the STD limit verified above. With the expressions in Table I, Eq. (69) becomes a polynomial equation of  $P$  that can be solved only with experimental parameters. The result given by this is shown in Fig. 7, which primarily provides a qualitative reference for the overall trends of optical pumping efficiency.

## C. Magnetic resonance enhancement

As described in Sec. III C 3, the performance of atomic magnetometers can be reflected in the magnetic resonance linewidth  $\Gamma_2$  and the maximum amplitude  $Y_{\text{max}}$ . And the optical shift  $\delta\Omega_L$  is also noticed. They are displayed in Fig. 8 to illustrate how different laser detunings enhance the magnetic resonance signal in the QHP regime.

In Fig. 8(a),  $\Gamma_2(\Delta_a = 0)$  and  $\Gamma_2(\Delta_b = 0)$  versus  $\Phi$  are compared. More than well-known light-narrowing effect [26], we

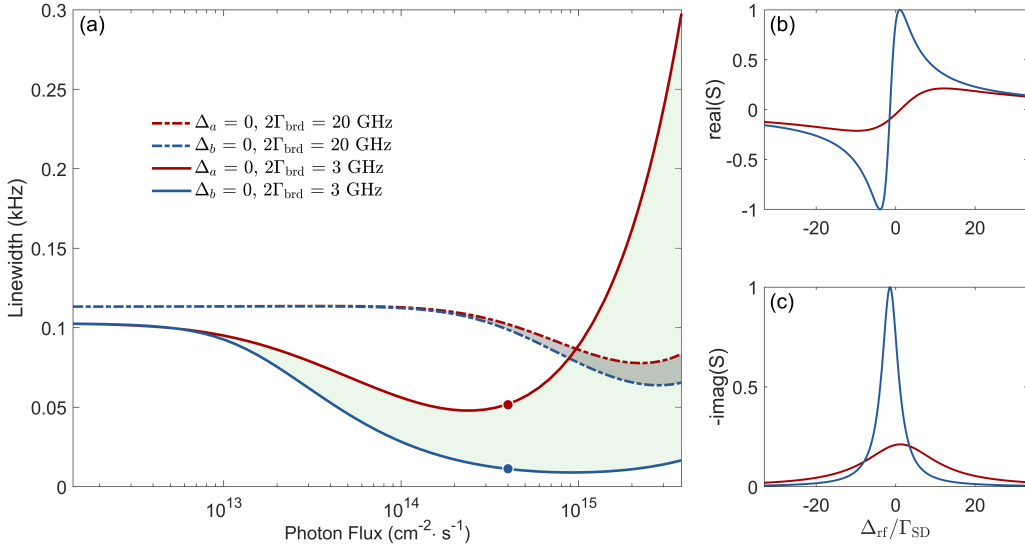


FIG. 8. (a) Magnetic resonance linewidth  $\Gamma_2$  (see Eq. 52) for different laser detunings and collisional broadening values. The shaded regions highlight the narrower linewidth that arises when the laser is resonant with the  $b$  multiplet. (b)–(c) show the normalized  $X$  and  $Y$  components in Eqs. (54) and (55), respectively, where the red and blue lines correspond to the marked points of the same colors in (a). The magnetic resonance signal at  $\Delta_b = 0$  exhibits a narrower linewidth and a stronger response. In above results,  $\Gamma_{\text{ex}}$  and  $\Gamma_{\text{SD}}$  correspond to  $^{87}\text{Rb}$  with  $\text{N}_2$  buffer gas at  $100^\circ\text{C}$ , and a weak field  $B = 5 \mu\text{T}$  is applied.

discover an extra narrowing effect induced by the resonant frequencies related to  $\Delta_F$  for  $F = a, b$

$$\Gamma_2(\Delta_a = 0) > \Gamma_2(\Delta_b = 0) \quad (71)$$

generally both in the light-narrowing and light-broadening regimes. And the difference gradually disappears with larger  $\Gamma_{\text{brd}}$  in the HP limit, although the underlying mechanism remains operative. The narrowing effect can be exemplified by  $\Gamma_2$  analytically derived in two polarization limits. In low polarization limit, the linewidth with first order correction is

$$\Gamma_2^{(P \rightarrow 0)} = q_{\text{ex}}(I)\Gamma_{\text{ex}} + q_{\text{SD}}(I)(\Gamma_{\text{SD}} + R_{\text{op}}Q_a) \quad (72)$$

where two slowing-down factors  $q_{\text{ex}}(I)$  and  $q_{\text{SD}}(I)$  are [19]

$$q_{\text{SD}}(I) = \frac{[I]^2}{2I^2 + I + 1}, \quad (73)$$

$$q_{\text{ex}}(I) = \frac{3[I]^2}{2I(2I - 1)}. \quad (74)$$

The traditional light-narrowing effect arises from higher order corrections including  $1/(R_{\text{op}}Q_a)$  term. In high polarization limit, the linewidth is dominant by

$$\Gamma_2^{(P \rightarrow 1)} = \frac{1}{[I]}R_{\text{op}}Q_a + \frac{1}{2}\Gamma_{\text{SD}}. \quad (75)$$

In both Eqs. (72) and Eq. (75), the optical pumping contribution is determined by  $R_{\text{op}}Q_a = \Phi A_0 \Gamma_{\text{brd}} / (\Delta_a^2 + \Gamma_{\text{brd}}^2)$ . Consequently, the cases of  $\Delta_a = 0$  and  $\Delta_b = 0$  result in additional broadening and narrowing, respectively. These behaviors originate from  $|\tilde{\rho}_1\rangle$  dynamics governed by  $\mathcal{G}_{\text{WDA}}$ , whose lowest eigenvalue in the  $a$ -subspace dominates  $\Gamma_2$ , as mentioned in Sec. III C.

The narrowing effect induced by optical resonance with the  $b$  multiplet significantly enhances the magnetic resonance signal, as is shown in Fig. 8(b) and Fig. 8(c). Evidently, compared with pumping at  $\Delta_a = 0$ , the response near  $\Delta_b = 0$  is markedly superior, exhibiting a narrower resonance peak together with a substantially stronger amplitude. Such behaviors can be approximated and explained by the maximum amplitude of the out-of-phase quadrature  $Y_{\text{max}} \sim P/\Gamma_2$ . For optical pumping in the QHP regime, there exists a regime of laser detuning in which increasing  $P$  leads to stronger coherence source for  $|\tilde{\rho}_1\rangle$ , and meanwhile  $\Gamma_2$  remains well protected or suppressed by the narrowing mechanism.

Additionally, the optical shift  $\delta\Omega_L$  of  $S$  described by Eq. (53) is included in Fig. 8. As an application, we emphasize that at the favored detuning  $\Delta_b = 0$

$$\delta\Omega_L(\Delta_b = 0) = \frac{1}{[I]} \frac{\Phi A_0 \omega_{\text{hf}}^{(g)}}{\delta_{\text{hf}}^2 + \Gamma_{\text{brd}}^2}. \quad (76)$$

which means that  $\delta\Omega_L$  can be avoided or minimized [27], at specific laser detunings without sacrifice of the magnetic resonance linewidth and amplitude.

## V. CONCLUSIONS

We developed a theoretical framework for optical pumping of alkali-metal atoms in buffer-gas cells in the QHP regime, where the collisional broadening  $\Gamma_{\text{brd}}$  is comparable to the GS hyperfine splitting, and far exceeds any other splitting or broadening. Via the master equation in Liouville space including various optical and collisional mechanisms, we studied optical pumping with the  $F = a$  and  $F = b$  hyperfine mul-

triplet resolved and establish a compact relation linking QHP superoperators to their HP counterparts, providing a unified theoretical framework. Moreover, we investigate the steady state beyond STD and point out the validity of the STD limit under typical conditions. To apply these treatments to atomic magnetometers, We further analyzed observables including the electron spin polarization, the absorption cross section and the magnetic resonance linewidth. Finally, We find and explain that in the QHP regime the magnetic resonance is significantly enhanced, exhibiting both linewidth narrowing and increased resonance amplitude at laser detuning near  $\Delta_b = 0$ .

In summary, our study provides a deep understanding of optical pumping in the QHP regime and offers useful theoretical tools with practical applicability to atomic sensors (e.g., atomic magnetometers), operating under realistic buffer-gas pressures. It also establishes a foundation for extending the present framework to incorporate additional physical effects, such as atomic diffusion.

## VI. ACKNOWLEDGMENTS

This work is supported by XXXX.

### Appendix A: BLOCKS IN LIOUVILLE SPACE

In Liouville-space calculations, an appropriate ordering of the basis states is essential for exposing the block structure of large superoperators. Such a decomposition not only improves computational efficiency but also highlights the underlying physical organization of the dynamics. In this Appendix, we introduce a block scheme constructed by grouping density-matrix elements according to their characteristic evolution frequencies [19], with emphasis on the blocks associated with the Zeeman subspaces.

The projection operator of the GS  $k$ th-order Zeeman coherence  $\mathcal{P}_Z^{(k)}$  is introduced as

$$\mathcal{P}_Z^{(k)} = \mathcal{P}_a^{(k)} + \mathcal{P}_b^{(k)}, \quad (\text{A1})$$

with  $\mathcal{P}_a^{(k)}$  and  $\mathcal{P}_b^{(k)}$  being that of  $F = a, b$  subspaces

$$\mathcal{P}_a^{(k)} = \sum_m |am + k; am\rangle \langle am + k; am|, \quad (\text{A2})$$

$$\mathcal{P}_b^{(k)} = \sum_m |bm - k; bm\rangle \langle bm - k; bm|. \quad (\text{A3})$$

where  $|Fm_F; F'm'_F\rangle$  is the basis of  $|\rho^{(\text{gg})}\rangle$  in Liouville space,

$$|Fm_F; F'm'_F\rangle = |Fm_F\rangle \langle F'm'_F|. \quad (\text{A4})$$

For an superoperator  $\mathcal{X}$ , its block  $[\mathcal{X}]_{m,n}$  is defined as

$$[\mathcal{X}]_{m,n} = \mathcal{P}_Z^{(m)} [\mathcal{X}] \mathcal{P}_Z^{(n)} \quad (\text{A5})$$

which couples  $n$ th-order to  $m$ th-order Zeeman coherence subspace. The zeroth-order Zeeman coherence is population.

To simplify the full dynamical evolution of  $|\rho^{(\text{gg})}\rangle$ , we neglect the coherences between hyperfine multiplets  $F = a, b$  and focus on mechanisms in the Zeeman Subspace, i.e.,  $\text{span}\{|Fm_F, Fm'_F\rangle\}$ . This is because in the absence of microwave driving, the hyperfine coherences will decay within a timescale typically on the order of approximately milliseconds or even shorter [28].

### Appendix B: THE OPTICAL SUPEROPERATORS IN THE QHP REGIME

In the QHP regime, we begin with the way to deal with the effective complex detuning  $\Delta + i\Gamma_{\text{brd}}$  and offer detailed proof for the  $\Delta_F$ -dependent form of superoperators  $\mathcal{A}_{\text{dp}}$  in Eqs. (25) and (26) and  $\mathcal{A}_p^{(\text{eg})}$  in Eq. (B15). Following calculations will utilize the identities in Liouville space [17]

$$\langle \mu' \nu' | A^b | \mu \nu \rangle = \langle \mu' | A | \mu \rangle \delta_{\nu \nu'}, \quad (\text{B1})$$

$$\langle \mu' \nu' | A^\# | \mu \nu \rangle = \delta_{\mu' \mu} \langle \nu | A | \nu' \rangle, \quad (\text{B2})$$

$$\langle \mu' \nu' | A^b B^\# | \mu \nu \rangle = \langle \mu' | A | \mu \rangle \langle \nu | B | \nu' \rangle. \quad (\text{B3})$$

with matrices  $A$  and  $B$  with column labels  $\mu, \nu$  and row labels  $\mu', \nu'$ . Using Eqs. (11), (B1) and (B2), the depopulation term  $\mathcal{A}_{\text{dp}}$  generally becomes

$$\mathcal{A}_{\text{dp}} = \frac{i[\mathcal{V}^\dagger \mathcal{V} / (\Delta + i\Gamma_{\text{brd}})]^b}{R_{\text{op}}} - \frac{i[\mathcal{V}^\dagger \mathcal{V} / (\Delta^T - i\Gamma_{\text{brd}}) \mathcal{V}]^\#}{R_{\text{op}}}, \quad (\text{B4})$$

where elements of the two terms above are

$$\begin{aligned} & \left( F' m_F'''; F' m_F'' \left| \frac{i[\mathcal{V}^\dagger \mathcal{V} / (\Delta + i\Gamma_{\text{brd}})]^b}{R_{\text{op}}} \right| F m_F'; F m_F \right) \\ &= \frac{i|\Omega_1|^2 / R_{\text{op}}}{\Delta_F + i\Gamma_{\text{brd}}} \left( F' m_F'''; F' m_F'' \left| \frac{1}{2} - \mathbf{s} \cdot \mathbf{S}^b \right| F m_F'; F m_F \right), \end{aligned} \quad (\text{B5})$$

and in the same way,

$$\begin{aligned} & \left( F' m_F'''; F' m_F'' \left| \frac{-i[\mathcal{V}^\dagger \mathcal{V} / (\Delta^T - i\Gamma_{\text{brd}}) \mathcal{V}]^\#}{R_{\text{op}}} \right| F m_F'; F m_F \right) \\ &= \frac{-i|\Omega_1|^2 / R_{\text{op}}}{\Delta_F - i\Gamma_{\text{brd}}} \left( F' m_F'''; F' m_F'' \left| \frac{1}{2} - \mathbf{s} \cdot \mathbf{S}^\# \right| F m_F'; F m_F \right), \end{aligned} \quad (\text{B6})$$

Here the  $D_1$  line identity  $e^* \cdot \mathbf{d} \mathbf{d}^\dagger \cdot e = 1/2 - \mathbf{s} \cdot \mathbf{S}$  is used again. Through Eqs (19) and (24), we see that

$$Q_F = \frac{|\Omega_1|^2 \Gamma_{\text{brd}} / R_{\text{op}}}{\Delta_F^2 + \Gamma_{\text{brd}}^2}. \quad (\text{B7})$$

It is emphasized that all the detuning dependence of  $\mathcal{A}_{\text{dp}}$  arises from the quantum number  $F$  of the coherence or population  $|Fm'_F; Fm_F\rangle$ . This allows us to simply introduce factors  $Q_F$  with  $F = a, b$  to respectively weight contributions of the hyperfine multiplets. Therefore, with the projection operators in

Eqs. (A1), (A2) and (A3), we can derive  $[\mathcal{A}_{\text{dp}}]_{mn}$

$$[\mathcal{A}_{\text{dp}}]_{m,n} = \sum_F Q_F \mathcal{P}_Z^{(m)} \text{Re} [\mathcal{A}_{\text{dp}}^{(\text{HP})}]_{m,n} \mathcal{P}_F^{(n)} + i \sum_F \frac{Q_F \Delta_F}{\Gamma_{\text{brd}}} \cdot \mathcal{P}_Z^{(m)} \text{Im} [\mathcal{A}_{\text{dp}}^{(\text{HP})}]_{m,n} \mathcal{P}_F^{(n)}. \quad (\text{B8})$$

where  $\mathcal{A}_{\text{dp}}^{(\text{HP})}$  is the depopulation term in the HP limit

$$\mathcal{A}_{\text{dp}}^{(\text{HP})} = 1 - \mathbf{s} \cdot (\mathbf{S}^\# + \mathbf{S}^\#) + i\mathbf{s} \cdot \mathbf{S}^\circ. \quad (\text{B9})$$

If the matrices  $Q_{\mathcal{L}}^{(k)}$  and  $\mathcal{K}_{\mathcal{L}}^{(k)}$  in Eq. (27) and (28) containing  $Q_F$  are introduced, we compactly rewrite the real and imaginary part of  $[\mathcal{A}_{\text{dp}}]_{m,n}$  as a column transformation to  $\text{Re} [\mathcal{A}_{\text{dp}}^{(\text{HP})}]_{m,n}$  and  $\text{Im} [\mathcal{A}_{\text{dp}}^{(\text{HP})}]_{m,n}$ , respectively. Thereafter, Eqs (25) and (26) is proved.

Similarly, we deal with the excitation transfer superoperator  $\mathcal{A}_{\text{p}}^{(\text{eg})}$ . Through Eq. (B15), it is generally

$$\mathcal{A}_{\text{p}}^{(\text{eg})} = -[\mathcal{V}./(\Delta + i\Gamma_{\text{brd}})]^{\text{b}} \mathcal{V}^{\dagger\#} + \mathcal{V}^{\text{b}} [\mathcal{V}^{\dagger}./(\Delta^{\text{T}} - i\Gamma_{\text{brd}})]^{\#}. \quad (\text{B10})$$

Using the property Eq. (B3), the elements are calculated below

$$\begin{aligned} & (\bar{F}\bar{m}'_F; \bar{F}\bar{m}_F | -[\mathcal{V}./(\Delta + i\Gamma_{\text{brd}})]^{\text{b}} \mathcal{V}^{\dagger\#} | Fm'_F; Fm_F) \\ &= -\frac{|\Omega_1|^2}{\Delta_F + i\Gamma_{\text{brd}}} \langle \bar{F}\bar{m}'_F | \mathbf{d}^\dagger \cdot \hat{\mathbf{e}} | Fm'_F \rangle \langle Fm_F | \mathbf{d} \cdot \hat{\mathbf{e}}^* | \bar{F}\bar{m}_F \rangle, \end{aligned} \quad (\text{B11})$$

and likewise

$$\begin{aligned} & (\bar{F}\bar{m}'_F; \bar{F}\bar{m}_F | \mathcal{V}^{\text{b}} [\mathcal{V}^{\dagger}./(\Delta^{\text{T}} - i\Gamma_{\text{brd}})]^{\#} | Fm'_F; Fm_F) \\ &= \frac{|\Omega_1|^2}{\Delta_F - i\Gamma_{\text{brd}}} \langle \bar{F}\bar{m}'_F | \mathbf{d}^\dagger \cdot \hat{\mathbf{e}} | Fm'_F \rangle \langle Fm_F | \mathbf{d} \cdot \hat{\mathbf{e}}^* | \bar{F}\bar{m}_F \rangle. \end{aligned} \quad (\text{B12})$$

We see the two terms in Zeeman subspace are Hermitian conjugate and hence their sum is

$$\begin{aligned} & (\bar{F}\bar{m}'_F; \bar{F}\bar{m}_F | \mathcal{A}_{\text{p}}^{(\text{eg})} | Fm'_F; Fm_F) \\ &= \frac{2|\Omega_1|^2 \Gamma_{\text{brd}}}{\Delta_F^2 + \Gamma_{\text{brd}}^2} \langle \bar{F}\bar{m}'_F | \mathbf{d}^\dagger \cdot \hat{\mathbf{e}} | Fm'_F \rangle \langle Fm_F | \mathbf{d} \cdot \hat{\mathbf{e}}^* | \bar{F}\bar{m}_F \rangle. \end{aligned} \quad (\text{B13})$$

With Eq. (B7), the block of  $\mathcal{A}_{\text{p}}^{(\text{eg})}$  in Zeeman subspace is

$$[\mathcal{A}_{\text{p}}^{(\text{eg})}]_{\bar{m},n} = \sum_F Q_F \mathcal{P}_Z^{(\bar{m})} [\mathcal{A}_{\text{p}}^{(\text{eg})(\text{HP})}]_{\bar{m},n} \mathcal{P}_F^{(n)}, \quad (\text{B14})$$

which is equivalent to Eq. (B15) with  $Q_{\mathcal{L}}^{(k)}$ . The excitation transfer term in the HP limit  $\mathcal{A}_{\text{p}}^{(\text{eg})(\text{HP})}$  is

$$\mathcal{A}_{\text{p}}^{(\text{eg})(\text{HP})} = 2(\hat{\mathbf{e}}^* \cdot \Delta^{\text{T}}) \otimes (\Delta^\dagger \cdot \hat{\mathbf{e}}), \quad (\text{B15})$$

In summary, it is proved that in the QHP regime, the optical superoperators  $\mathcal{A}_{\text{dp}}$  and  $\mathcal{A}_{\text{p}}^{(\text{eg})}$  both take the similar form i.e., the superoperator in the HP limit followed by the matrices whose elements vary with  $\Delta_F$ . Analysis in Sec. III C will present  $\mathcal{A}_{\text{op}}$  follow the same way as well.

- 
- [1] Y.-Y. Jau, A. B. Post, N. N. Kuzma, A. M. Braun, M. V. Romalis, and W. Happer, *Phys. Rev. Lett.* **92**, 110801 (2004).  
[2] J. Vanier and C. Audoin, *The Quantum Physics of Atomic Frequency Standards* (A. Hilger, Philadelphia, 1989).  
[3] D. Budker and M. Romalis, *Nature Physics* **3**, 227 (2007).  
[4] D. Budker and D. F. J. Kimball, *Optical Magnetometry* (Cambridge University Press, Cambridge, UK, 2013).  
[5] J. Fang and J. Qin, *Sensors* **12**, 6331 (2012).  
[6] M. J. Wright, L. Anastassiou, C. Mishra, J. M. Davies, A. M. Phillips, S. Maskell, and J. F. Ralph, *Front. Phys.* **10**, 994459 (2022).  
[7] T. G. Walker and M. S. Larsen, *Adv. At. Mol. Opt. Phys.* **65**, 373 (2016).  
[8] G. Gao, J. Hu, F. Tang, W. Liu, X. Zhang, B. Wang, D. Deng, M. Zhu, and N. Zhao, *Phys. Rev. Appl.* **21**, 014042 (2024).  
[9] W. Happer, *Rev. Mod. Phys.* **44**, 169 (1972).  
[10] S. J. Seltzer, Developments in alkali-metal atomic magnetometry, Ph.d. thesis, Princeton University (2008).  
[11] S. J. Seltzer and M. V. Romalis, *Journal of Applied Physics* **106**, 114905 (2009).  
[12] M. E. Wagshul and T. E. Chupp, *Phys. Rev. A* **49**, 3854 (1994).  
[13] B. Lancor and T. G. Walker, *Phys. Rev. A* **82**, 043417 (2010).  
[14] J. Lu, S. Zhang, Y. Zhou, Y. Yan, F. Lu, K. Wang, Y. Zhai, and M. Ye, *Sensors and Actuators A: Physical* **347**, 113928 (2022).  
[15] Y. Jia, Z. Liu, Z. Chai, X. Liang, and W. Wu, *IEEE Trans. Instrum. Meas.* **70**, 1 (2021).  
[16] J. Vanier, *Appl. Phys. B* **81**, 421 (2005).  
[17] W. Happer, Y. Y. Jau, and T. Walker, *Optically Pumped Atoms* (Wiley, New York, 2010).  
[18] T. G. Walker and W. Happer, *Rev. Mod. Phys.* **69** (1997).  
[19] F. Tang and N. Zhao, *Phys. Rev. A* **111**, 013103 (2025).  
[20] W. Happer and A. C. Tam, *Phys. Rev. A* **16**, 1877 (1977).  
[21] I. M. Savukov and M. V. Romalis, *Phys. Rev. A* **71**, 023405 (2005).  
[22] K. Ishikawa and T. Yabuzaki, *Phys. Rev. A* **62**, 065401 (2000).  
[23] S. Appelt, A. B.-A. Baranga, C. J. Erickson, M. V. Romalis, A. R. Young, and W. Happer, *Phys. Rev. A* **58**, 1412 (1998).  
[24] F. P. Kelly, *Reversibility and Stochastic Networks* (Cambridge University Press, Cambridge, UK, 2011).  
[25] W. Happer and B. S. Mathur, *Phys. Rev. Lett.* **18**, 577 (1967).  
[26] S. Appelt, A. Ben-Amar Baranga, A. R. Young, and W. Happer, *Phys. Rev. A* **59**, 2078 (1999).  
[27] Y. Chang, Y.-H. Guo, and J. Qin, *Phys. Rev. A* **99**, 063411 (2019).  
[28] E. P. Corsini, T. Karaulanov, M. Balabas, and D. Budker, *Phys. Rev. A* **87**, 022901 (2013).